

1 Evaluation of the nemabiome approach for the study of

2 equine strongylid communities

3

4 Élise Courtot^{1,*}, Michel Boisseau^{1,2,*}, Sophie Dhorne-Pollet³, Delphine Serreau¹, Amandine
5 Gesbert⁴, Fabrice Reigner⁴, Marta Basiaga⁵, Tetiana Kuzmina⁶, Jérôme Lluch⁷, Gwenolah
6 Annonay⁷, Claire Kuchly⁷, Irina Diekmann⁸, Jürgen Krücken⁸, Georg von Samson-
7 Himmelstjerna⁸, Nuria Mach^{2,‡}, Guillaume Sallé^{1,‡}

8

9 1, Université de Tours, INRAE, UMR1282 ISP, 37380 Nouzilly, France

10 2, IHAP, Université de Toulouse, INRAE, ENVT, Toulouse Cedex 3, 31076, France

11 3, Université Paris-Saclay, INRAE, AgroParisTech, GABI, 78350 Jouy-en-Josas, France

12 4, INRAE, UE PAO, 37380 Nouzilly, France

13 5, Department of Zoology and Animal Welfare, Faculty of Animal Science, University of Agriculture in
14 Kraków, 24/28 Mickiewicza Av., 30-059 Kraków, Poland

15 6, Department of Parasitology I. I. Schmalhausen Institute of Zoology NAS of Ukraine, Kyiv, Ukraine

16 7, GeT-PlaGe, INRAE, Genotoul, Castanet-Tolosan, France

17 8, Freie Universität Berlin, Institute for Parasitology and Tropical Veterinary Medicine, Berlin, Germany

18 *‡, both authors contributed equally to this work

19

20 Corresponding author

21 Guillaume SALLÉ

22 INRAE Centre Val de Loire, 37380 Nouzilly, FRANCE

23 Email address: guillaume.salle@inrae.fr

24 **Abstract**

25 Basic knowledge on the biology and epidemiology of equine strongylid species remains
26 insufficient although it would contribute to the design of better parasite control strategies.

27 Nemabiome is a convenient tool to quantify and to identify species in bulk samples that could
28 overcome the hurdle that cyathostomin morphological identification represents. To date, this
29 approach has relied on the internal transcribed spacer 2 (ITS-2) of the ribosomal RNA cistron
30 and its predictive performance and associated biases both remain unaddressed.

31 This study aimed to bridge this knowledge gap using cyathostomin mock communities and
32 comparing performances of the ITS-2 and a *cytochrome c oxidase subunit I* (COI) barcode newly
33 developed in this study. The effects of bioinformatic parameters were investigated to determine
34 the best analytical pipelines. Subsequently, barcode predictive abilities were compared across
35 various mock community compositions. The replicability of the approach and the amplification
36 biases of each barcode were estimated. Results were also compared between various types of
37 biological samples, i.e. eggs, infective larvae or adults.

38 Overall, the proposed COI barcode was suboptimal relative to the ITS-2 rDNA region, because
39 of PCR amplification biases, a reduced sensitivity and higher divergence from the expected
40 community composition. Metabarcoding yielded consistent community composition across the
41 three sample types, although infective larvae may remain the most tractable in the field.

42 Additional strategies to improve the COI barcode performances are discussed. These results
43 underscore the critical need of mock communities for metabarcoding purposes.

44 Introduction

45 Equine strongylids encompass a diverse fauna of 14 Strongylinae and 50 Cyathostominae
46 described species (Lichtenfels et al., 2008). Among these, species from the genus *Strongylus* are
47 responsible for the death of animals because of verminous arteritis liver pathology and peritonitis
48 while Cyathostominae impinge on their host growth (McCraw and Slocombe, 1985, 1978, 1976;
49 Reinemeyer and Nielsen, 2009). In addition, the mass emergence of developing cyathostomin
50 stages can lead to a fatal syndrome of cyathostominosis characterized by abdominal pain,
51 diarrhea or fever (Giles et al., 1985). The release of modern anthelmintics has drastically reduced
52 the prevalence of *Strongylus* sp in the field as first mentioned in 1990 (Herd, 1990) and later
53 confirmed by observations from necropsy data (Lyons et al., 2000; Sallé et al., 2020). However,
54 treatment failure against cyathostomins has been found on many occasions across every
55 continent for all drug classes currently available (Peregrine et al., 2014). Despite their worldwide
56 distribution and relevance for stakeholders in the field, little knowledge has been gathered on the
57 mechanisms driving their assemblage. Recent meta-analyses found that strongylid community
58 structure was little affected by geo-climatic factors (Bellaw and Nielsen, 2020; Boisseau et al.,
59 2021; Louro et al., 2021) and a few observations exist on the relationship between cyathostomin
60 assemblage structure and environmental factors like temperature (Kuzmina et al., 2006; Nielsen
61 et al., 2007), horse age (Bucknell et al., 1995; Kuzmina et al., 2016; Torbert et al., 1986) or the
62 host sex (Kornas et al., 2010; Sallé et al., 2018). The tedious and delicate process of species
63 identification by morphological keys (Lichtenfels et al., 2008) is a major hurdle to study further
64 the mechanisms of species assemblage, their turnover and the respective impacts of the host and
65 their environment.

66 DNA-metabarcoding is a non-invasive, time- and cost-effective method for assessing nematode
67 populations that provides data with comparable taxonomic resolution to morphological methods
68 (Avramenko et al., 2015). This requires appropriate barcodes able to distinguish between the
69 various phylogenetic strata. The internal transcribed spacer 2 region (ITS-2) of the nuclear rRNA
70 cistron (Blouin, 2002; Kiontke et al., 2011) and the mitochondrial COI gene (Blaxter et al., 2005;
71 Blouin, 2002; Prosser et al., 2013) have already been used for nematode molecular barcoding.
72 For cyathostomin species, early barcoding attempts relied on the polymorphisms present in the
73 ITS-2 rDNA region (Hung et al., 2000, 1999) before additional contributions were made using
74 COI gene (McDonnell et al., 2000), or the longer intergenic spacer sequence (Cwiklinski et al.,
75 2012). Additional work recently highlighted how the COI region could increase the resolution of
76 species genetic diversity, suggesting a close phylogenetic relationship between *Coronocyclus*
77 *coronatus* and *Cylicostephanus calicatus* (Bredtmann et al., 2019; Louro et al., 2021). In addition
78 to this higher resolutive power, the protein-coding nature of the COI barcode can be leveraged to
79 denoise sequencing data (Ramirez-Gonzalez et al., 2013). To date, metabarcoding experiments
80 on equine strongylid species have exclusively focused on the ITS-2 rDNA cistron (Poissant et
81 al., 2021). This may owe to the existence of universal primers and the length of the amplicon that
82 is a good fit for short-read sequencing platforms. Observations in helminths also suggest that
83 amplification efficiency is suboptimal for the COI region (Prosser et al., 2013) which speaks
84 against its application for metabarcoding purposes. However, mitochondrial markers have better
85 discriminating abilities between closely related or cryptic species (Bredtmann et al., 2019; Gao et
86 al., 2020; Louro et al., 2021). Hence, the added value of the COI barcode remains to be
87 determined for the study of cyathostomin species.

88 In addition, nemabiome approaches are biased in predicting relative taxon abundances (McLaren
89 et al., 2019). These biases are inherent to various biological and technical factors including the
90 DNA treatment procedures, the different number of cells represented by each taxon (that is
91 tightly linked to the life-stage considered for strongylid species), PCR specifications (cycle
92 number) and the amplification efficiency across taxa, and the genetic diversity (including
93 structural variants and copy numbers) of the considered barcodes within taxa (Pollock et al.,
94 2018). To date, the precision and recall of the metabarcoding approach applied to cyathostomins
95 are unresolved. It is also currently unknown whether this approach provides a fair description of
96 the actual species presence or absence, or their accurate relative abundances in their host. The
97 impact of the considered life-stage, *i.e.* eggs, larvae or adult worms, has not been studied yet.
98 Here, we aimed to address these three questions, i) the added value of the COI barcode to
99 describe cyathostomin populations from mock samples in horses, ii) the predictive ability of the
100 nemabiome approach to provide comparable results to morphological identification and iii)
101 whether strongylid species can be correctly detected from different strongylid life-stages.
102 For this purpose, we developed degenerated primers to amplify the COI region following a
103 strategy successful under other settings (Elbrecht et al., 2019; Elbrecht and Leese, 2017a), we
104 built mock communities of diverse equine strongylid species and applied a nemabiome approach
105 targeting the ITS-2 rDNA and COI gene regions. We compared the predictive performances of
106 both approaches for various analytical pipelines and across diverse sample types and
107 demonstrated that the ITS-2 rDNA barcode is a more reliable predictor of horses cyathostomin
108 community taxonomical structure than the proposed COI barcode. Still, bioinformatic parameters
109 need careful evaluation and amplification biases across species were found. For both barcodes,
110 similar results were obtained from cyathostomin eggs, larvae or adult stages suggesting limited

111 biases induced by the sample type. In conclusion, this study underscores the need for mock
112 communities when studying equine strongylid communities with a metabarcoding approach.

113

114 **Materials and methods**

115 **Mock community design and DNA extraction**

116 Mock communities were built from morphologically identified equine strongylid specimens from
117 pooled fecal samples in Ukraine (Kuzmina et al., 2016) and Poland. For each species, a single
118 adult male was digested using proteinase K (Qiagen) in lysis buffer, before DNA extraction
119 using a phenol/chloroform protocol. DNA was precipitated overnight in ethanol and sodium
120 acetate (5M) at -20°C and washed twice with 70% ethanol. The resulting DNA pellet was
121 resuspended in 30 µL of TE buffer (10 mM Tris-HCl, 0.1 mM EDTA, pH 8.0) and DNA was
122 quantified using the Qubit® double-stranded high sensitivity assay kit (Life
123 Technologies™) with a minimal sensitivity of 0.1 ng/µL. Extracted DNA was stored at -20°C.
124 To quantify the impact of the community complexity, mock communities of 11 and five species
125 were built and subjected to amplicon sequencing using the ITS-2 rDNA and mitochondrial COI
126 barcodes (Table 1). Within each community, species DNA was either added on an equimolar
127 basis or at their respective concentrations to mimic differences occurring in the field
128 (heterogeneous communities; Table 1). Of note, the homogeneous communities comprised two
129 *Cyathostomum pateratum* individuals to assess the impact of inter-individual variation. To
130 further measure the resolution ability of the nemabiome approach, two-species communities
131 were made with *Cyathostomum catinatum* and *C. pateratum*. Both species were either in
132 imbalanced ratios (3-fold difference in both directions) or equal DNA concentration.

133

134

135 **Table 1. Detailed mock community composition**

Mock community composition Available replicates/barcode	Species (input DNA concentration; Fraction of total DNA amount)
Homogeneous, 11 species ITS-2: 1 ; COI: 2	<ul style="list-style-type: none">• <i>Cyathostomum pateratum</i> (0.27 ng/µL; 16.7%) ;• Others (0.135 ng/µL ; 8.3%):<ul style="list-style-type: none">◦ <i>Cylicocyclus ashworthi</i>, <i>Cylicocyclus insigne</i>, <i>Cylicocyclus leptostomum</i>, <i>Cylicocyclus nassatus</i> ;◦ <i>Coronocyclus labratus</i>, <i>Coronocyclus labiatus</i> ;◦ <i>Cylicostephanus calicatus</i>, <i>Cylicostephanus goldi</i>, <i>Cylicostephanus longibursatus</i>;◦ <i>Cyathostomum catinatum</i>,
Heterogeneous, 11 species ITS-2: 1 ; COI: 2	<ul style="list-style-type: none">• <i>C. ashworthi</i> (0.553 ng/µL; 4.6%), <i>C. insigne</i> (1.06 ng/µL; 11.2%), <i>C. leptostomus</i> (0.549 ng/µL; 8.8%), <i>C. nassatus</i> (1.28 ng/µL; 10.7%);• <i>C. labratus</i> (0.251 ng/µL; 2.1%), <i>C. labiatus</i> (0.498 ng/µL; 42.8%);• <i>C. calicatus</i> (0.216 ng/µL; 4.6%), <i>C. goldi</i> (0.135 ng/µL; 9%), <i>C. longibursatus</i> (1.34 ng/µL; 4.1%);• <i>C. pateratum</i> (5.14 ng/µL; 1.1%), <i>C. catinatum</i> (1.08 ng/µL; 1%)
Homogeneous, five species* ITS-2: 2 ; COI: 2	<i>C. pateratum</i> (4 ng/µL; 33.3%); Others (2 ng/µL; 16.7%): <i>C. insigne</i> , <i>C. nassatus</i> , <i>C. labiatus</i> , <i>C. catinatum</i>
Heterogeneous, five species* ITS-2: 2 ; COI: 2	<i>C. insigne</i> (3.73 ng/µL; 4.1%), <i>C. nassatus</i> (1.07 ng/µL; 11.6%); <i>C. labiatus</i> (1.52 ng/µL; 16.5%); <i>C. catinatum</i> (0.64 ng/µL; 6.9%), <i>C. pateratum</i> (5.61 ng/µL; 64.82%)
Homogeneous, two species ITS-2: 2 ; COI: 1	<i>C. catinatum</i> (0.5 ng/µL ; 25%), <i>C. pateratum</i> (3.5 ng/µL ; 75%)
Homogeneous, two species, low concentration ; ITS-2: 2 ; COI: 1	<i>C. catinatum</i> (0.135 ng/µL; 50%), <i>C. pateratum</i> (0.135 ng/µL; 50%)
One-to-four ratio, two species ITS-2: 2 ; COI: 1	<i>C. catinatum</i> (3 ng/µL ; 75%), <i>C. pateratum</i> (1 ng/µL ; 25%)
Three-to-four ratio, two species ITS-2: 2 ; COI: 1	<i>C. catinatum</i> (1 ng/µL; 25%), <i>C. pateratum</i> (3 ng/µL; 75%)

136

137 The detailed composition of the eight mock communities used in this study is provided with the
138 respective final DNA concentration and relative abundance of each species. The number of replicate
139 libraries is provided for each barcode (ITS-2 rDNA and COI). Asterisks mark the two mock communities
140 used to compare the predictive abilities of each barcode and to estimate the replicability of the approach.

141

142

143

144

145 **Parasite material collection for comparison of the metabarcoding performances across**
146 **sample type**

147 Parasite material was collected from six Welsh ponies with patent strongylid infection. Faecal
148 matter (200 g) was recovered from the rectum and incubated with 30% vermiculite at 25°C and
149 60% humidity for 12 days, before third-stage larvae were recovered using a Baerman apparatus.
150 Strongylid eggs were extracted from another 200g of faeces. For this, faecal matter was placed
151 onto a coarse sieve to remove large plant debris, before further filtering was made on finer sieves
152 (150 μ M and 20 μ M mesh). Kaolin (Sigma K7375) was then added (0.5% w/v) to the egg
153 suspension to further pellet contaminating debris (5 min centrifugation at 2,000 rpm). The
154 supernatant was discarded and the egg pellet was resuspended in a dense salt solution (NaCl, d =
155 1.18) and centrifuged slowly (1,200 rpm for 5 min), before this final egg suspension was placed
156 on a 20 μ M mesh sieve for a last wash. Adult worms were collected from the same ponies at 18
157 and 21 hours after a pyrantel embonate treatment (Strongid[®], Zoetis, France; 6.6 mg/Kg body
158 weight). DNA extraction was performed as for the mock community samples. The amounts of
159 adult worms, infective larvae and eggs are listed in Table 2.

160

161

162 **Table 2: Quantity of larvae, adults and eggs used for DNA extractions. The quantities indicated are**
163 **those present in each faecal aliquot.**

Host tag	Adults worms	Infective Larvae	Number of eggs
W646	50	17,500	36,000
W710	50	24,000	43,000
W729	50	21,000	35,000
W733	17	20,000	35,000
W734	50	12,000	35,000
W748	50	27,000	35,000

164
165 For every test sample collected from six Welsh ponies, the quantities of recovered parasite material is
166 indicated for each type of biological material recovered.

167

168 **COI and ITS-2 primer design**

169 We aimed to define a 450-bp amplicon within the 650-bp fragment of the cytochrome c oxidase
170 subunit I (COI) locus previously described (Bredtmann et al., 2019; Louro et al., 2021). This
171 would leave at most 50 bp overlap, thereby allowing sequencing error correction and better
172 amplicon resolution (Edgar and Flyvbjerg, 2015). For this, the mitochondrial sequences of 18
173 cyathostomin species with complete mitochondrial genomes available at that time (October 9th,
174 2020) were considered (AP017681: *Cylicostephanus goldi*, AP017698: *Strongylus vulgaris*;
175 GQ888712: *Cylicocyclus insigne*; Q888717: *Strongylus vulgaris*; NC_026729: *Triodontophorus*
176 *brevicauda*; NC_026868: *Strongylus equinus*; NC_031516: *Triodontophorus serratus*;
177 NC_031517: *Triodontophorus nipponicus*; NC_032299: *Cylicocyclus nassatus*; NC_035003:
178 *Cyathostomum catinatum*; NC_035004: *Cylicostephanus minutus*; NC_035005: *Poteriostomum*
179 *imparidentatum*; NC_038070: *Cyathostomum pateratum*; NC_039643: *Cylicocyclus radiatus*;

180 NC_042141: *Cylicodontophorus bicoronatus*; NC_042234: *Coronocyclus labiatus*; NC_043849:
181 *Cylicocyclus auriculatus*; NC_046711: *Cylicocyclus ashworthi*). These sequences were aligned
182 with Muscle v.3.8.21 (Edgar, 2004). Subsequently, this alignment was used to quantify sequence
183 heterozygosity for 450-bp sliding windows using a custom python script (supplementary file S1).
184 The consensus sequence of the region with the highest diversity, *i.e.* best discriminant across
185 species, was isolated to design primers with the Primer3 blast web-based interface (Untergasser
186 et al., 2012). Parameters were chosen to have an amplicon product of 400-450 bp, primers of 20
187 bp with melting temperatures of $60^{\circ}\text{C} \pm 1^{\circ}\text{C}$. Primer sequences were subsequently degenerated to
188 account for identified SNPs in the mitochondrial sequence alignment, yielding a 24-bp long
189 forward (5'-RGCHAARCCNGGDYTRTTRYTDGG-3') and 25-bp long reverse (5'-
190 GYTCYAAHGAAATHGAHCTHCTHCG-3') primers. For the ITS-2 barcode, we relied on
191 previously described primers (5'-ACGTCTGGTTCAGGGTTGTT-3') and NC2 (5'-
192 TTAGTTCTTTCCTCCGCT-3') applied on cyathostomin communities already (Gasser et al.,
193 1993). In both cases, a random single, double or triple nucleotide was added to the 5' primer end
194 to promote sequence complexity and avoid signal saturation. A 28-bp Illumina overhang was
195 added for the forward and reverse sequences respectively, for subsequent ligation with Illumina
196 adapters.

197

198 **Library preparation and sequencing**

199 For library preparation, PCR reactions were carried out in 80 μl with 16 μl HF buffer 5X, 1.6 μl
200 dNTPs (10mM), 4 μl primer mix containing forward and reverse primers, 0.8 μl Phusion High-
201 Fidelity DNA Polymerase (2U/ μl , Thermo Scientific), and 10 ng of genomic DNA. PCR
202 conditions for ITS-2 were 95°C for 3 min for the first denaturation, then 30 cycles at 98°C for 15

203 s, 60°C for 15 s, 72°C for 15 s, followed by a final extension of 72°C for 2 min. For COI
204 amplification, the PCR parameters were 95°C for 3 min, followed by a pre-amplification with 5
205 cycles of 98°C for 15 s, 45°C for 30 s, 72°C for 30 s, followed by 35 cycles of 98°C for 15 s,
206 55°C for 30 s, 72°C for 30 s then a final extension of 2 min at 72°C.

207 For each sample, 20 µl were examined on 1% agarose gel to check for the presence of a PCR
208 amplification band at the expected product size (or absence thereof for negative controls). The
209 concentrations of the purified amplicons were checked using a NanoDrop 8000
210 spectrophotometer (Thermo Fisher Scientific, Waltham, USA), and the quality of a set of
211 amplicons was checked using DNA 7500 chips onto a Bioanalyzer 2100 (Agilent Technologies,
212 Santa Clara, CA, USA). A homemade six-bp index was added to the reverse primer during a
213 second PCR with 12 cycles using forward primer
214 (AATGATAACGGCGACCACCGAGATCTACACTCTTCCCTACACGAC) and reverse
215 primer (CAAGCAGAAGACGGCATACGAGAT-index-GTGACTGGAGTTCAGACGTGT)
216 for single multiplexing. The final libraries had a diluted concentration of 5 nM to 20 nM and
217 were used for sequencing. Amplicon libraries were mixed with 15% PhiX control for quality
218 check. Libraries were further processed for a single run of MiSeq sequencing using the 500-cycle
219 reagent kit v3 (2 x 250 output; Illumina, USA).

220

221 **Analytical pipelines**

222 *Quality control and filtering*

223 Sequencing data were first filtered using cutadapt v1.14 to remove insufficient quality data (-q
224 15), trim primer sequences, and remove sequences with evidence of indels (--no-indels) or that
225 showing no trace of primer sequence (--discard-untrimmed).

226 *Analytical pipelines for community structure inference using the ITS-2 amplicon*

227 The implemented framework was similar to previous work (Poissant et al., 2021) that used the
228 DADA2 algorithm (Callahan et al., 2016) to identify amplicon sequencing variants after error
229 rate learning and correction. The denoising procedure, consisting in learning error rates
230 independently for both forward and reverse reads, was applied for two discrete stringency
231 parameter sets either tolerating a single error for both reads (mxEE = 1) or more relaxed
232 stringency (mxEE = 2 and 5 for the forward and reverse reads respectively). Truncation length of
233 forward and reverse reads was set to 200 or 217 bp. Last, the band_size parameter effect was
234 also explored considering three values, i.e. -1, 16 and 32, that respectively disable banding and
235 implement the default or a more relaxed value that is recommended for ITS-2 sequences. In
236 every case, denoising was run using the pseudo-pool option and chimera detection relied on the
237 consensus mode.

238 Taxonomic assignment was subsequently performed using a sequence composition approach
239 using the IDTAXA algorithm (Murali et al., 2018) as implemented in the DECIPHER R package
240 v.2.18.1 with minimal bootstrap support of 50%. This last step relied on the curated ITS-2 rDNA
241 database for nematodes (Workentine et al., 2020), last accessed on February 3rd 2022.

242

243

244 *Analytical pipelines for community structure inference using the COI amplicon*

245 For the COI barcode, we built a custom COI barcode sequence database for Cyathostominae and
246 Strongylidae species collected from Genbank, BOLD database using the Primerminer package
247 v.0.18 (Elbrecht and Leese, 2017b) and concatenated into a single fasta file. Sequences were
248 subsequently edited to remove elephant Cyathostominae species (*Quilonia* sp, *Murshidia* sp,

249 *Kilonia* sp, and *Milulima* sp) using the seqtk v.1.3 subseq option (<https://github.com/lh3/seqtk>).
250 Some entry names (n = 18) consisted of an accession number that was manually back-
251 transformed to the corresponding species name. Duplicate entries were removed with the rmdup
252 option of the seqkit software v.0.16.0 (Shen et al., 2016) and sequences were dereplicated using
253 the usearch v11.0.667 -fastx_uniques option (Edgar, 2010). To reduce the database complexity
254 and promote primary alignment, the most representative sequences were further determined
255 using the usearch -cluster_smallmem option, considering two identity thresholds of 97 and 99%.
256 Amplicon analysis relied on a mapping approach to the custom COI sequence database
257 implemented using the minimap2 software v.2-2.11 (Li, 2018) as described elsewhere (Ji et al.,
258 2020). First, paired-end reads were merged into amplicon sequences using the usearch software
259 v11.0.667 and the -fastq_mergelpair option (Edgar, 2010). Merged amplicon sequences were
260 subsequently mapped onto the COI sequence database using the minimap2 short read mode (-ax
261 sr) (Li, 2018). Mapping stringency was varied to select the most appropriate combinations using
262 k-mer sizes of 10, 13, and 15 (default), window sizes w of 8, 9 or 10 (default), and varying
263 mismatch penalty values (B = 1, 2, 3 or the default values 4). The lower the value, the more
264 permissive the alignment for these three parameters. Produced alignments were converted to bam
265 files using samtools v1-10 after filtering against unmapped reads, alignments that were not
266 primary and supplementary secondary alignments using the -F 2308 flag (Li et al., 2009). To
267 evaluate how mapping stringency, filtered bam files were also produced using a mapping quality
268 cut-off of 30. Species abundance was then inferred from read depth over each COI sequence that
269 was determined using the bedtools genomecov algorithm (Quinlan and Hall, 2010) and scaled by
270 the sequence length.

271

272 **Quantitative PCR (qPCR) assay for species-specific amplification of the ITS-2 rDNA**
273 **region**

274 To quantify any biases in PCR amplification, single-species DNA used to make mock
275 communities was subjected to quantitative PCR reactions with the ITS-2 and COI-specific
276 primers. The DNA was diluted at 1:250 and 1 μ l of DNA was added to each reaction. qPCRs
277 were carried out on a Biorad CFX Connect Real-Time PCR Detection System following the iQ
278 SYBR GREEN supermix® protocol (Biorad, France, 1708882). Reactions were run in triplicate
279 for each species with 40 amplification cycles: 95°C for 3 min for the first denaturation, then 45
280 cycles of 98°C for 15 s, 60°C for 30 s, 72°C for 40 s, followed by a melt curve (65°C to 95°C).

281

282 **Statistical analyses**

283 Statistical analyses were run with R v.4.0.2 (R Core Team, 2016). Community compositional
284 data were imported and handled with the phyloseq package v1-34.0 (McMurdie and Holmes,
285 2013). Abundance data (read count for the ITS-2 rDNA region, or scaled read depth for COI)
286 were aggregated at the species level using the *taxglom()* function of the phyloseq package v1-
287 34.0 and converted to relative abundances for further analysis. These data were used to compare
288 the predictive ability of each barcode and pipeline in a first comparison. After the best
289 bioinformatics parameters were identified for each barcode, the ASV count tables were further
290 filtered to remove putative contaminants or spurious signals representing either less than 100
291 reads per base pair for the COI barcode or 40 reads for the ITS-2 rDNA barcodes.

292 Species richness, alpha-diversity and beta-diversity analyses were conducted with the vegan
293 package v2.5-7 (Oksanen et al., 2017). PerMANOVA was implemented using the *adonis()*
294 function of the vegan package v2.5-7 (Oksanen et al., 2017).

295 To monitor the predictive ability of each pipeline and barcode, the precision (the proportion of
296 true positives among all positives called, i.e. true positives and false positives) and recall (the
297 proportion of true positives among all true positives, i.e. true positives and false negatives) of the
298 derived community species composition were computed and combined into the F1-score as:

$$F1 = 2 \times \frac{recall \times precision}{recall + precision}$$

300 This score supports the ability of a method to correctly identify species presence while
301 minimizing the number of false-positive predictions (trade-off between precision and recall)
302 (Hleap et al., 2021).

303 Alpha diversity was estimated using the Shannon and Simpson's indices using the
304 *estimate_richness()* function of the phyloseq package (McMurdie and Holmes, 2013). To
305 compare between conditions and barcodes, the difference between the mock community
306 expected and observed alpha diversity values was further considered. The divergence between
307 the inferred community species composition and the true mock community composition was
308 estimated from a between-community distance matrix based on species presence/absence
309 (Jaccard distance) or species relative abundances (Bray-Curtis dissimilarity) using the *vegdist()*
310 function of the vegan package (Oksanen et al., 2017). Differences in nemabiome between sample
311 types were visualized with a non-metric multidimensional scaling (NMDS) with two dimensions
312 using Jaccard and Bray-Curtis dissimilarity.

313 For each of these variables (F1-score, alpha-diversity differences and divergence) and within
314 each barcode, estimated values were regressed upon bioinformatics pipeline parameters (mxee,
315 truncation length and band size parameters for the ITS-2 barcode data; k-mer size, window size,
316 mismatch penalty and mapping quality for the COI barcode) to estimate the relative contribution
317 of these parameters and determine the most appropriate combination for each barcode

318 independently. The model with the lowest Akaike Information Criterion value was first selected
319 with the *stepAIC()* function of the R MASS package v.7.3-55 (Venables and Ripley, 2002) to
320 retain the most relevant parameter combination (model with the lowest AIC). Parameter values
321 were then chosen according to their least-square mean estimate. These analyses were applied to
322 every available data within each barcode.

323 These variables were subsequently compared between the ITS-2 and COI barcodes using the best
324 bioinformatic pipeline and across every community available for each barcode. Replicability was
325 estimated from the two mock communities with five species, available for both barcodes (Table
326 1) and the contribution of species and replicate run effects were determined using the same AIC-
327 based procedure.

328 To estimate amplification efficiencies, the threshold cycle (Ct) values were regressed upon the
329 log10-transformed DNA concentration for each species and barcode. The PCR efficiency was

330 subsequently derived as: $E_{i,j} = 10^{-\frac{1}{\beta_{i,j}}}$, where $E_{i,j}$ is the efficiency, and $\beta_{i,j}$ stands for the
331 regression slope of species i and barcode j . The R script and the necessary files used for analysis
332 are available under the github repository at
333 https://github.com/guiSalle/Horse_Nemabiome_benchmark. The associated raw sequencing will
334 be made available upon manuscript acceptance on the SRA platform.

335

336 **Results**

337 **Impact of the community size on the ITS-2 and COI barcode performances**

338 The best bioinformatic parameters were determined for each barcode according to their
339 predictive performances of mock community composition (Supplementary information and
340 supplementary Tables 1, 2 and 3). This comparison relied on the same two mock communities of
341 five species (Table 1). The combination of the minimap default values for the mismatch penalty
342 ($B = 4$) and the window size ($w = 10$) parameters, with a k-mer size of 10 base pairs and no
343 further filtering on mapping quality ($MQ = 0$) was deemed as the most optimal pipeline for the
344 COI barcode. For ITS-2, stringent tolerance in the maximal expected number of errors and a
345 truncation length of 200 bp was the best parameters for cyathostomin community structure
346 prediction.

347 With these settings, the number of reads available for the considered mock communities ranged
348 between 6,164 and 151,606 reads for the COI barcode, while these numbers ranged between 816
349 and 86,424 non-chimeric sequences for the ITS-2 rDNA barcode.

350 No significant difference was found in the F1 score between the ITS-2 and COI barcodes ($F_{1,19} =$
351 0.26, $P = 0.61$; Figure 1). In terms of species detection, the COI barcode ability to recover the
352 true species composition was suboptimal: this barcode recovered nine correct species at most in
353 the most complex communities and systematically overlooked *C. leptostomum* and *C. labratus* in
354 these. On the contrary, it also identified *C. coronatus* (in all of the four 11-species mock
355 communities) and *C. minutus* (in one out of the four 11-species mock communities) despite these
356 species not being present. Their relative abundances remained however lower than 1% for *C.*
357 *coronatus* and 0.02% for *C. minutus* and was associated with low mapping quality (Phred quality

358 score < 6). The ITS-2 rDNA barcode performed better with ten species detected overall but *C.*
359 *goldi* was systematically overlooked in the 11-species mock communities.

360 The ITS-2 barcode gave better representations of the most complex cyathostomin communities
361 composition (with five or eleven species; Figure 1B, C). for species relative abundances
362 (reduction of 0.14 ± 0.07 in Bray-Curtis dissimilarity relative to COI, $P = 0.04$) or species
363 presence/absence (decrease of 0.18 ± 0.08 in Jaccard distance relative to COI, $P = 0.04$). The
364 ITS-2 barcode also gave the closest estimates of the expected alpha diversity ($F_{1,19} = 22.9$, $P =$
365 1.2×10^{-4} and $F_{1,19} = 34.9$, $P < 10^{-4}$ for Simpson and Shannon indices; Figure 1). These
366 differences vanished however when considering the mock communities composed of two
367 *Cyathostomum* species (Figure 1): no statistical difference was found in any of the six parameters
368 in that case ($P > 0.2$ in all cases).

369 Last, the fraction of unassigned reads increased with the mock community size for the ITS-2
370 rDNA barcode (ranged between 17% to 35%, Figure 1) but remained negligible with the COI
371 region as a result of the mapping procedure (2×10^{-5} % for the most complex community and
372 null otherwise; Figure 1).

373 In summary, none of the two barcodes offered a perfect fit for the expected community
374 composition, but the ITS-2 rDNA barcode was closer to the truth.

375

376 **377 Replicability and correspondence between read counts and input DNA for the ITS-2 and
COI barcodes**

378 Pearson's correlation between log-transformed species abundance measured across two runs for
379 two 5-species mock communities (Table 1) was 98% for both barcodes. In line with this
380 consistency across libraries, input DNA concentration modeling performed best when using the
381 observed read counts and species as predictors (model AIC = 15.8 and 27.9; $R^2 = 87.3\%$ and

382 73.9% for ITS-2 and COI barcodes). The replicate effect was negligible in both cases ($F_{1,17} =$
383 0.2, $P = 0.66$ and $F_{1,17} = 0.001$, $P = 0.99$ for the ITS-2 and COI respectively; Figure 2).
384 Despite similar behaviours in terms of modeling species DNA abundance, the correlation
385 between observed read counts and species input DNA quantity was 75% for the ITS-2 rDNA
386 barcode but non-significantly different from 0 for the COI barcode (Pearson's $r = -0.21$, $P =$
387 0.38; Figure 2).
388 Hence, the designed COI barcode appeared suboptimal in its ability to provide a fair
389 representation of the input cyathostomin DNA abundance, in sharp contrast with the ITS-2
390 barcode.

391

392 **PCR amplification bias for the COI and ITS-2 rDNA barcodes**

393 The imperfect correlations found between input DNA quantity and observed read counts might
394 relate to biases in the first PCR amplification. To test this hypothesis, qPCRs were performed on
395 each species DNA from the same single individual used for library preparation (Table 3). The
396 average amplification efficiency was $67.7\% \pm 0.24\%$ for the COI barcode. It was above 90% for
397 the two *Cyathostomum* species (Table 3) but it fell below 70% for five species. Among these, *C.*
398 *calicatus* and *C. longibursatus* showed the lowest values (39% and 13% respectively, Table 3).
399 Omitting the outlier values found for the *Cylicostephanus* members (*C. goldi* undetected and too
400 high efficiency for *C. calicatus*; Table 3), the ITS-2 rDNA barcode yielded more consistent and
401 higher amplification efficiency on average ($92.2\% \pm 0.03\%$; $t_{10} = 3.42$, $P = 0.006$) than COI.

402

403

404 **Table 3. Species-specific amplification efficiencies of the COI and ITS-2 barcodes for 11**
 405 **cyathostomin species**

Barcode	Genus	Species	Slope	Std. error	Intercept	Efficiency	R ²
COI	<i>Coronocyclus</i>	<i>C. labratus</i>	-3.90	0.52	-1.48	0.81	0.87
		<i>C. labiatus</i>	-4.70	0.44	-5.12	0.63	0.93
	<i>Cyathostomum</i>	<i>C. pateratum</i>	-3.45	0.55	1.90	0.95	0.82
		<i>C. catinatum</i>	-3.53	0.22	2.70	0.92	0.97
	<i>Cylicocyclus</i>	<i>C. leptostomum</i>	-3.98	0.45	-3.93	0.78	0.91
		<i>C. ashworthi</i>	-4.34	0.35	-3.92	0.70	0.95
		<i>C. nassatus</i>	-4.36	0.47	-5.32	0.70	0.91
		<i>C. insigne</i>	-4.38	0.39	-5.30	0.69	0.94
		<i>C. calicatus</i>	-6.99	0.71	20.89	0.39	0.92
	<i>Cylicostephanus</i>	<i>C. goldi</i>	-3.98	1.91	29.73	0.78	0.29
		<i>C. longibursatus</i>	-19.06	3.77	-7.28	0.13	0.89
ITS-2	<i>Coronocyclus</i>	<i>C. labratus</i>	-3.48	0.11	14.47	0.94	0.99
		<i>C. labiatus</i>	-3.53	0.13	15.93	0.92	0.99
	<i>Cyathostomum</i>	<i>C. pateratum</i>	-3.33	0.13	15.91	1.00	0.99
		<i>C. catinatum</i>	-3.64	0.14	15.18	0.88	0.99
	<i>Cylicocyclus</i>	<i>C. leptostomum</i>	-3.47	0.07	14.24	0.94	1.00
		<i>C. ashworthi</i>	-3.49	0.13	15.63	0.94	0.99
		<i>C. nassatus</i>	-3.43	0.11	15.57	0.95	0.99
		<i>C. insigne</i>	-3.43	0.12	15.36	0.96	0.99
		<i>C. calicatus</i>	-3.64	0.08	14.41	0.88	1.00
	<i>Cylicostephanus</i>	<i>C. goldi</i>	0.00	0.40	33.09	-1.00	-0.06
		<i>C. longibursatus</i>	-0.98	0.88	26.65	9.53	0.03

406
 407 Regression coefficients (slope, associated standard error and intercept) of the amplification efficiency
 408 (measured with Ct) upon DNA concentration are given for every cyathostomin species considered.
 409 Derived amplification efficiency and regression explanatory power are also provided. Data are ordered by
 410 genus and efficiency.

411

412

413

414 **The considered life stage has limited effect on the inference of community composition**

415 Nemabiome data were generated from six horses for three life stages (eggs, infective larvae and
416 adult worms collected after pyrantel treatment). The total number of species present in this
417 population remains unknown to date. The COI barcode retrieved 12 species, of which *C.*
418 *radiatus* was not found with the ITS-2 barcode. This latter barcode allowed the retrieval of 13
419 species and four additional amplicon sequence variants that were assigned at the genus level only
420 (Figure 3). ITS-2 data also recovered *C. leptostomum* and *Craterostomum acuticaudatum* that
421 were not found with the COI marker (Figure 3).

422

423 **Table 4. Shannon index estimated using three sample types**

Type	Barcode	Average \pm standard error
Eggs	COI	0.58 \pm 0.36
L3	COI	0.65 \pm 0.32
Pool	COI	0.58 \pm 0.46
Eggs	ITS-2	1.11 \pm 0.47
L3	ITS-2	0.93 \pm 0.66
Pool	ITS-2	1.10 \pm 0.62

424 For each sample type, the average Shannon index estimated across six replicates and associated standard
425 error is provided.

426

427 The Shannon index showed no significant variation across the considered life-stages for both
428 barcodes ($P = 0.96$, Table 4) as the observed differences fell below the resolute power of this
429 experiment (difference of 1.8 detectable with a significance level of 5% and power of 80%).

430 Alpha-diversity estimates obtained with the ITS-2 barcode were higher (difference of 0.44 ± 0.16
431 relative to COI, $t_1 = 2.75, P = 0.01$; Table 4).

432 The community structure was generally in good agreement across sample types for both the ITS-
433 2 and COI barcodes, although two larval samples exhibited outlying behaviours with the ITS-2
434 barcode (Figure 3). In agreement with this observation, PerMANOVA showed that the sample
435 type was not a significant driver of the beta-diversity, explaining 16.8% ($P = 0.12, F_{2,15} = 1.51$,
436 $R^2 = 0.168$) and 9.9% ($P = 0.63, F_{2,15} = 0.83, R^2 = 0.099$) of the variance in species relative
437 abundances for the COI and ITS-2 barcode respectively.

438 Altogether, these observations suggest that metabarcoding would yield the same results from
439 cyathostomin eggs extracted from the faecal matter, infective larvae harvested after egg culture
440 or adult worm collection after treatment.

441

442 **Discussion**

443 This study proposed a new barcode based on the COI gene and quantified the effect of a few
444 factors affecting the metabarcoding of horse strongylid communities, including bioinformatic
445 pipeline parameters, the number of species in the community, the barcode amplification step or
446 the considered sample type. Overall, the proposed COI barcode appears suboptimal in
447 comparison to the ITS-2. The use of a mock community is of utmost importance to fine tune the
448 bioinformatic pipeline parameters while the approach appears to be robust across the various
449 sample types available.

450 The COI region has been used for nemabiome or phylogenetic studies of other nematode species,
451 including *Haemonchus contortus* (Blouin, 2002) or some free-living *Caenorhabditis* species
452 (Kiontke et al., 2011). Its higher genetic variation poses this marker as an ideal barcode for
453 cyathostomin species with evidence that it could better delineate the phylogenetic relationship
454 between *Coronocyclus coronatus* and *Cylicostephanus calicatus* members (Louro et al. 2021).
455 This study aimed to produce amplicons suitable for merging of read pairs, i.e. with a total length
456 lower than 500 bp. To compensate for the diversity found across species over that region, primer
457 sequences were degenerated and a 5-cycle at lower temperature pre-amplification was applied to
458 compensate for suboptimal priming (Kwok et al., 1994) while subsequent mapping stringency
459 was lowered to promote read mapping against the reference sequence database. As can be
460 expected, this strategy yielded a poor correlation between input DNA and quantified reads.
461 Specifically, the PCR amplification efficiency showed significant variation across species with
462 suboptimal amplification for *C. calicatus* and *C. longibursatus* species. Additional factors such
463 as the type of DNA polymerase could also affect the results and warrant further investigations
464 (Nichols et al., 2018). The designed COI barcode did not outperform the ITS-2 rDNA region in

465 terms of species detection or Jaccard-based (species presence or absence) diversity estimates. In
466 this respect, inclusion of *C. coronatus* in mock communities may have yielded less favourable
467 results for the ITS-2 rDNA barcode as this species entertains close phylogenetic relationship
468 with *C. calicatus* (Bredtmann et al., 2019).

469 While the described approach was suboptimal, other strategies targeting the mitochondrial
470 genome could still be applied (Ji et al., 2020; Liu et al., 2016). First, bulk shotgun sequencing of
471 cyathostomin populations could be used for mapping against a reference database of
472 mitogenomes as applied to arthropods (Ji et al., 2020). This strategy improved the correlation
473 between species input DNA and the number of mapped reads (Ji et al., 2020). This is however
474 more expensive and is limited by the available mitogenomic resources for equine strongylids (18
475 species available at the time of this experiment). Primer cocktail to simultaneously amplify
476 multiple amplicons is another alternative that may increase the range of diversity being sampled
477 (Chase and Fay, 2009). However, its performance under other settings was poor and was not
478 better than relying on degenerated primers (Elbrecht et al., 2019). Last, third-generation
479 sequencing technologies like the Pacific Biosciences and Oxford Nanopore Technologies which
480 are both able to sequence long DNA fragments, could recover the whole COI gene or the
481 mitochondrial genome from a pool of strongylid species. The portable Oxford Nanopore
482 Technologies device offers a convenient set-up that can be deployed in the field (Quick et al.,
483 2015), and could deliver full-length COI barcode data for up to 500 insect specimens in a single
484 run (Srivathsan et al., 2018). This comes, however, at the cost of sequencing errors associated
485 with insertion/deletion errors over homopolymeric regions (Srivathsan et al., 2018). But this
486 drawback can be overcome as the protein-coding nature of the COI gene provides a solid basis
487 for error denoising (Andújar et al., 2018; Ramirez-Gonzalez et al., 2013).

488 The ITS-2 rDNA region has been implemented already for characterizing equine strongylid
489 communities (Poissant et al., 2021) but its predictive performances have not been characterized
490 against mock equine strongylid communities. Its amplification was more robust as already
491 reported (Louro et al., 2021) and the PCR amplification efficiency was consistent across
492 considered species. The lower amplification found for the two *Cylicostephanus* species mirrored
493 that found with COI and may relate to the input material. It remains unclear however why the
494 recorded amplifications were slightly lower for *C. catinatum* and *C. calicatus*. The presence of
495 polymorphisms in the latter species has been described and could have hampered PCR
496 amplification (Louro et al., 2021).

497 Despite the breadth of species considered in this work, it was not possible to cover every known
498 member of the equine Cyathostominae and Strongylidae families. Past investigation has focused
499 on *Strongylus* spp showing that the metabarcoding was underestimating their true abundances
500 (Poissant et al., 2021). Among the Cyathostominae family, species of intermediate abundance
501 and prevalence like *C. coronatus* and *C. radiatus* should be considered for further studies.
502 Specifically, the ability of the various approaches and algorithms to delineate between *C.*
503 *calicatus* and *C. coronatus* members should be further investigated. As our observations suggest
504 that pipeline performances were dependent on the species number, an investigation of more
505 complex communities remains to be completed.

506 In turn, nemabiome is expected to unravel yet unknown facets of cyathostomin phenology, like
507 their seasonal preference, or any priority effects between species (Boisseau et al., 2021). The
508 lack of significant differences between the considered sample types for this approach supports a
509 flexible implementation in the field. Infective larvae certainly can be harvested a few days after
510 sample collection and as such, they remain the most convenient sample type for field work. In

511 contrast, egg samples will develop into first-stage larvae within 24–48 hours and adult collection
512 will be dependent on the species drug sensitivity.
513 To overcome the described challenges owing to barcode properties, metagenomic shotgun
514 sequencing on DNA extracted from faeces could resolve the horse gut biodiversity in a single-
515 pot experiment. While gut microbial gene catalogs have been built recently (Ang et al., 2022;
516 Mach et al., 2022), the genomic resources for cyathostomin remain restricted to a few
517 mitochondrial genomes that span the *Coronocyclus* (Yang et al., 2020), *Cyathostomum* (Wang et
518 al., 2020), *Cylicocyclus* (Y. Gao et al., 2017), *Cylicostephanus* (Gao et al., 2020), and
519 *Triodontophorus* (J.-F. Gao et al., 2017) genera, and a single heavily fragmented genome
520 assembly for *C. goldi* (International Helminth Genomes, 2019).

521 Conclusion

522 This work investigated the impact of experimental factors on metabarcoding approaches applied
523 to equine strongylids. Overall, the developed COI barcode was suboptimal relative to the ITS-2
524 region. But this latter barcode displayed variable PCR amplification efficiency that may bias
525 subsequent inferences. Cyathostomin larvae appear to be the most valuable biological material
526 for metabarcoding. However, reliance on eggs extracted from the faecal matter or adult worms
527 yielded the same results and could be considered for studies.
528 Metagenomic sequencing should offer a viable option to overcome the limitations of barcodes
529 but is faced with limited available genomic resources for the species of interest.

530 Acknowledgements

531 The authors are grateful to the INRAE UEPAO equine facility for their support in implementing
532 this experiment. We are grateful to the genotoul bioinformatics platform Toulouse Occitanie
533 (Bioinfo Genotoul, <https://doi.org/10.15454/1.5572369328961167E12>) for providing computing
534 and storage resources.

535 References

536 Andújar, C., Arribas, P., Yu, D.W., Vogler, A.P., Emerson, B.C., 2018. Why the COI barcode
537 should be the community DNA metabarcode for the metazoa. *Mol Ecol* 27, 3968–3975.
538 <https://doi.org/10.1111/mec.14844>

539 Ang, L., Vinderola, G., Endo, A., Kantanen, J., Jingfeng, C., Binetti, A., Burns, P., Qingmiao, S.,
540 Suying, D., Zuijiang, Y., Rios-Covian, D., Mantziari, A., Beasley, S., Gomez-Gallego, C.,
541 Gueimonde, M., Salminen, S., 2022. Gut Microbiome Characteristics in feral and
542 domesticated horses from different geographic locations. *Commun Biol* 5, 172.
543 <https://doi.org/10.1038/s42003-022-03116-2>

544 Avramenko, R.W., Redman, E.M., Lewis, R., Yazwinski, T.A., Wasmuth, J.D., Gilleard, J.S.,
545 2015. Exploring the Gastrointestinal “Nemabiome”: Deep Amplicon Sequencing to
546 Quantify the Species Composition of Parasitic Nematode Communities. *PLoS One* 10,
547 e0143559. <https://doi.org/10.1371/journal.pone.0143559>

548 Bellaw, J.L., Nielsen, M.K., 2020. Meta-analysis of cyathostomin species-specific prevalence
549 and relative abundance in domestic horses from 1975-2020: emphasis on geographical
550 region and specimen collection method. *Parasit Vectors* 13, 509.
551 <https://doi.org/10.1186/s13071-020-04396-5>

552 Blaxter, M., Mann, J., Chapman, T., Thomas, F., Whitton, C., Floyd, R., Abebe, E., 2005.
553 Defining operational taxonomic units using DNA barcode data. *Phil. Trans. R. Soc. B*
554 360, 1935–1943. <https://doi.org/10.1098/rstb.2005.1725>

555 Blouin, M.S., 2002. Molecular prospecting for cryptic species of nematodes: mitochondrial DNA
556 versus internal transcribed spacer. *Int J Parasitol* 32, 527–531.
557 [https://doi.org/10.1016/s0020-7519\(01\)00357-5](https://doi.org/10.1016/s0020-7519(01)00357-5)

558 Boisseau, M., Mach, N., Basiaga, M., Kornaś, S., Kuzmina, T., Laugier, C., Sallé, G., 2021.
559 Species turnover between age groups of horses and positive network of co-occurrences
560 define the structure of horse strongylid communities: a meta-analysis. *BioRxiv*.
561 <https://doi.org/10.1101/2021.05.17.441725>

562 Bredtmann, C.M., Krücken, J., Kuzmina, T., Louro, M., Madeira de Carvalho, L.M., von
563 Samson-Himmelstjerna, G., 2019. Nuclear and mitochondrial marker sequences reveal
564 close relationship between *Coronocyclus coronatus* and a potential *Cylicostephanus*
565 *calicatus* cryptic species complex. *Infect Genet Evol* 75, 103956.
566 <https://doi.org/10.1016/j.meegid.2019.103956>

567 Bucknell, D.G., Gasser, R.B., Beveridge, I., 1995. The prevalence and epidemiology of
568 gastrointestinal parasites of horses in Victoria, Australia. *Int J Parasitol* 25, 711–24.

569 Callahan, B.J., McMurdie, P.J., Rosen, M.J., Han, A.W., Johnson, A.J.A., Holmes, S.P., 2016.
570 DADA2: High-resolution sample inference from Illumina amplicon data. *Nature Methods*
571 13, 581–583. <https://doi.org/10.1038/nmeth.3869>

572 Chase, M.W., Fay, M.F., 2009. Barcoding of Plants and Fungi. *Science* 325, 682–683.
573 <https://doi.org/10.1126/science.1176906>

574 Cwiklinski, K., Kooyman, F.N., Van Doorn, D.C., Matthews, J.B., Hodgkinson, J.E., 2012. New
575 insights into sequence variation in the IGS region of 21 cyathostomin species and the
576 implication for molecular identification. *Parasitology* 139, 1063–73.
577 <https://doi.org/10.1017/S0031182012000467>

578 Edgar, R.C., 2010. Search and clustering orders of magnitude faster than BLAST. *Bioinformatics*
579 26, 2460–2461. <https://doi.org/10.1093/bioinformatics/btq461>

580 Edgar, R.C., 2004. MUSCLE: multiple sequence alignment with high accuracy and high
581 throughput. *Nucleic Acids Res* 32, 1792–7. <https://doi.org/10.1093/nar/gkh340>

582 Edgar, R.C., Flyvbjerg, H., 2015. Error filtering, pair assembly and error correction for next-
583 generation sequencing reads. *Bioinformatics* 31, 3476–3482.
584 <https://doi.org/10.1093/bioinformatics/btv401>

585 Elbrecht, V., Braukmann, T.W.A., Ivanova, N.V., Prosser, S.W.J., Hajibabaei, M., Wright, M.,
586 Zakharov, E.V., Hebert, P.D.N., Steinke, D., 2019. Validation of COI metabarcoding
587 primers for terrestrial arthropods. *PeerJ* 7, e7745. <https://doi.org/10.7717/peerj.7745>

588 Elbrecht, V., Leese, F., 2017a. Validation and Development of COI Metabarcoding Primers for
589 Freshwater Macroinvertebrate Bioassessment. *Front. Environ. Sci.* 5.
590 <https://doi.org/10.3389/fenvs.2017.00011>

591 Elbrecht, V., Leese, F., 2017b. PrimerMiner \square : an r package for development and *in silico*
592 validation of DNA metabarcoding primers. *Methods Ecol Evol* 8, 622–626.
593 <https://doi.org/10.1111/2041-210X.12687>

594 Gao, J.-F., Liu, G.-H., Duan, H., Gao, Y., Zhang, Y., Chang, Q.-C., Fang, M., Wang, C.-R.,
595 2017. Complete mitochondrial genomes of *Triodontophorus serratus* and
596 *Triodontophorus nipponicus*, and their comparison with *Triodontophorus brevicauda*.
597 *Exp Parasitol* 181, 88–93. <https://doi.org/10.1016/j.exppara.2017.08.002>

598 Gao, Y., Qiu, J.-H., Zhang, B.-B., Su, X., Fu, X., Yue, D.-M., Wang, C.-R., 2017. Complete
599 mitochondrial genome of parasitic nematode *Cylicocyclus nassatus* and comparative
600 analyses with *Cylicocyclus insigne*. *Exp Parasitol* 172, 18–22.
601 <https://doi.org/10.1016/j.exppara.2016.11.005>

602 Gao, Y., Qiu, Y.-Y., Meng, X.-Q., Yang, X., Zhang, Z.-H., Diao, Z.-Y., Wang, S., Wang, C.-R.,
603 Song, M.-X., 2020. Comparative analysis of mitochondrial DNA datasets indicates that
604 *Cylicostephanus minutus* represents a species complex. *Infect Genet Evol* 84, 104487.
605 <https://doi.org/10.1016/j.meegid.2020.104487>

606 Gasser, R.B., Chilton, N.B., Hoste, H., Beveridge, I., 1993. Rapid sequencing of rDNA from
607 single worms and eggs of parasitic helminths. *Nucleic Acids Res* 21, 2525–2526.
608 <https://doi.org/10.1093/nar/21.10.2525>

609 Giles, C.J., Urquhart, K.A., Longstaffe, J.A., 1985. Larval cyathostomiasis (immature
610 trichonema-induced enteropathy): a report of 15 clinical cases. *Equine Vet J* 17, 196–201.

611 Herd, R.P., 1990. The changing world of worms: the rise of the cyathostomes and the decline of
612 *Strongylus vulgaris*. *Compendium on Continuing Education for the Practicing*

613 Veterinarian 12, 732–734.
614 Hleap, J.S., Littlefair, J.E., Steinke, D., Hebert, P.D.N., Cristescu, M.E., 2021. Assessment of
615 current taxonomic assignment strategies for metabarcoding eukaryotes. Molecular
616 Ecology Resources 21, 2190–2203. <https://doi.org/10.1111/1755-0998.13407>
617 Hung, G.C., Chilton, N.B., Beveridge, I., Gasser, R.B., 2000. A molecular systematic framework
618 for equine strongyles based on ribosomal DNA sequence data. Int J Parasitol 30, 95–103.
619 [https://doi.org/10.1016/s0020-7519\(99\)00166-6](https://doi.org/10.1016/s0020-7519(99)00166-6)
620 Hung, G.-C., Gasser, R.B., Beveridge, I., Chilton, N.B., 1999. Species-specific amplification by
621 PCR of ribosomal DNA from some equine strongyles. Parasitology 119, 69–80.
622 <https://doi.org/10.1017/S0031182099004497>
623 International Helminth Genomes, C., 2019. Comparative genomics of the major parasitic worms.
624 Nat Genet 51, 163–174. <https://doi.org/10.1038/s41588-018-0262-1>
625 Ji, Y., Huotari, T., Roslin, T., Schmidt, N.M., Wang, J., Yu, D.W., Ovaskainen, O., 2020.
626 SPIKEPIPE: A metagenomic pipeline for the accurate quantification of eukaryotic
627 species occurrences and intraspecific abundance change using DNA barcodes or
628 mitogenomes. Mol Ecol Resour 20, 256–267. <https://doi.org/10.1111/1755-0998.13057>
629 Kiontke, K.C., Félix, M.-A., Ailion, M., Rockman, M.V., Braendle, C., Pénigault, J.-B., Fitch,
630 D.H.A., 2011. A phylogeny and molecular barcodes for *Caenorhabditis*, with numerous
631 new species from rotting fruits. BMC Evol Biol 11, 339. <https://doi.org/10.1186/1471-2148-11-339>
632 Kornaś, S., Cabaret, J., Skalska, M., Nowosad, B., 2010. Horse infection with intestinal
633 helminths in relation to age, sex, access to grass and farm system. Vet Parasitol 174, 285–91.
634 <https://doi.org/10.1016/j.vetpar.2010.09.007>
635 Kuzmina, T.A., Dzeverin, I., Kharchenko, V.A., 2016. Strongylids in domestic horses: Influence
636 of horse age, breed and deworming programs on the strongyle parasite community. Vet
637 Parasitol 227, 56–63. <https://doi.org/10.1016/j.vetpar.2016.07.024>
638 Kuzmina, T.A., Kuzmin, Y.I., Kharchenko, V.A., 2006. Field study on the survival, migration
639 and overwintering of infective larvae of horse strongyles on pasture in central Ukraine.
640 Vet Parasitol 141, 264–72. <https://doi.org/10.1016/j.vetpar.2006.06.005>
641 Kwok, S., Chang, S.Y., Sninsky, J.J., Wang, A., 1994. A guide to the design and use of
642 mismatched and degenerate primers. PCR Methods Appl 3, S39–47.
643 <https://doi.org/10.1101/gr.3.4.s39>
644 Li, H., 2018. Minimap2: pairwise alignment for nucleotide sequences. Bioinformatics 34, 3094–
645 3100. <https://doi.org/10.1093/bioinformatics/bty191>
646 Li, H., Handsaker, B., Wysoker, A., Fennell, T., Ruan, J., Homer, N., Marth, G., Abecasis, G.,
647 Durbin, R., Genome Project Data Processing, S., 2009. The Sequence Alignment/Map
648 format and SAMtools. Bioinformatics 25, 2078–9.
649 <https://doi.org/10.1093/bioinformatics/btp352>
650 Lichtenfels, J.R., Kharchenko, V.A., Dvojnos, G.M., 2008. Illustrated identification keys to
651 strongylid parasites (Strongylidae: Nematoda) of horses, zebras and asses (Equidae). Vet
652 Parasitol 156, 4–161. <https://doi.org/10.1016/j.vetpar.2008.04.026>
653 Liu, S., Wang, X., Xie, L., Tan, M., Li, Z., Su, X., Zhang, H., Misof, B., Kjer, K.M., Tang, M.,
654 Niehuis, O., Jiang, H., Zhou, X., 2016. Mitochondrial capture enriches mito-DNA 100
655 fold, enabling PCR-free mitogenomics biodiversity analysis. Mol Ecol Resour 16, 470–
656 479. <https://doi.org/10.1111/1755-0998.12472>
657 Louro, M., Kuzmina, T.A., Bredtmann, C.M., Diekmann, I., de Carvalho, L.M.M., von Samson-
658

659 Himmelstjerna, G., Krücken, J., 2021. Genetic variability, cryptic species and
660 phylogenetic relationship of six cyathostomin species based on mitochondrial and nuclear
661 sequences. *Sci Rep* 11, 8245. <https://doi.org/10.1038/s41598-021-87500-8>

662 Lyons, E.T., Swerczek, T.W., Tolliver, S.C., Bair, H.D., Drudge, J.H., Ennis, L.E., 2000.
663 Prevalence of selected species of internal parasites in equids at necropsy in central
664 Kentucky (1995-1999). *Vet. Parasitol.* 92, 51–62.

665 Mach, N., Midoux, C., Leclercq, S., Pennarun, S., Le Moyec, L., Rué, O., Robert, C., Sallé, G.,
666 Barrey, E., 2022. The first horse gut microbiome gene catalog reveals that rare
667 microbiome ensures better cardiovascular fitness in endurance horses.
668 <https://doi.org/10.1101/2022.01.24.477461>

669 McCraw, B.M., Slocombe, J.O., 1985. *Strongylus equinus*: development and pathological effects
670 in the equine host. *Can J Comp Med* 49, 372–383.

671 McCraw, B.M., Slocombe, J.O., 1978. *Strongylus edentatus*: development and lesions from ten
672 weeks postinfection to patency. *Can J Comp Med* 42, 340–356.

673 McCraw, B.M., Slocombe, J.O., 1976. *Strongylus vulgaris* in the horse: a review. *Can Vet J* 17,
674 150–157.

675 McDonnell, A., Love, S., Tait, A., Lichtenfels, J.R., Matthews, J.B., 2000. Phylogenetic analysis
676 of partial mitochondrial cytochrome oxidase c subunit I and large ribosomal RNA
677 sequences and nuclear internal transcribed spacer I sequences from species of
678 Cyathostominae and Strongylinae (Nematoda, Order Strongylida), parasites of the horse.
679 *Parasitology* 121 Pt 6, 649–59.

680 McLaren, M.R., Willis, A.D., Callahan, B.J., 2019. Consistent and correctable bias in
681 metagenomic sequencing experiments. *eLife* 8, e46923.
682 <https://doi.org/10.7554/eLife.46923>

683 McMurdie, P.J., Holmes, S., 2013. phyloseq: An R Package for Reproducible Interactive
684 Analysis and Graphics of Microbiome Census Data. *PLoS ONE* 8, e61217.
685 <https://doi.org/10.1371/journal.pone.0061217>

686 Murali, A., Bhargava, A., Wright, E.S., 2018. IDTAXA: a novel approach for accurate
687 taxonomic classification of microbiome sequences. *Microbiome* 6, 140.
688 <https://doi.org/10.1186/s40168-018-0521-5>

689 Nichols, R.V., Vollmers, C., Newsom, L.A., Wang, Y., Heintzman, P.D., Leighton, M., Green,
690 R.E., Shapiro, B., 2018. Minimizing polymerase biases in metabarcoding. *Mol Ecol
691 Resour* 18, 927–939. <https://doi.org/10.1111/1755-0998.12895>

692 Nielsen, M.K., Kaplan, R.M., Thamsborg, S.M., Monrad, J., Olsen, S.N., 2007. Climatic
693 influences on development and survival of free-living stages of equine strongyles:
694 implications for worm control strategies and managing anthelmintic resistance. *Vet J* 174,
695 23–32. <https://doi.org/10.1016/j.tvjl.2006.05.009>

696 Oksanen, J., Blanchet, F.G., Friendly, M., Kindt, R., Legendre, P., McGlinn, D., Minchin, P.R.,
697 O'Hara, R.B., Simpson, G., Solymos, P., Stevens, M.H.H., Szoecs, E., Wagner, B.R.H.,
698 2017. vegan: Community Ecology Package. R package version 2.4-3.

699 Peregrine, A.S., Molento, M.B., Kaplan, R.M., Nielsen, M.K., 2014. Anthelmintic resistance in
700 important parasites of horses: does it really matter? *Vet Parasitol* 201, 1–8.
701 <https://doi.org/10.1016/j.vetpar.2014.01.004>

702 Poissant, J., Gavriliuc, S., Bellaw, J., Redman, E.M., Avramenko, R.W., Robinson, D.,
703 Workentine, M.L., Shury, T.K., Jenkins, E.J., McLoughlin, P.D., Nielsen, M.K., Gilleard,
704 J.S., 2021. A repeatable and quantitative DNA metabarcoding assay to characterize

705 mixed strongyle infections in horses. *Int J Parasitol* 51, 183–192.
706 <https://doi.org/10.1016/j.ijpara.2020.09.003>

707 Pollock, J., Glendinning, L., Wisedchanwet, T., Watson, M., 2018. The Madness of Microbiome:
708 Attempting To Find Consensus “Best Practice” for 16S Microbiome Studies. *Appl
709 Environ Microbiol* 84. <https://doi.org/10.1128/AEM.02627-17>

710 Prosser, S.W.J., Velarde-Aguilar, M.G., León-Règagnon, V., Hebert, P.D.N., 2013. Advancing
711 nematode barcoding: a primer cocktail for the cytochrome c oxidase subunit I gene from
712 vertebrate parasitic nematodes. *Mol Ecol Resour* 13, 1108–1115.
713 <https://doi.org/10.1111/1755-0998.12082>

714 Quick, J., Ashton, P., Calus, S., Chatt, C., Gossain, S., Hawker, J., Nair, S., Neal, K., Nye, K.,
715 Peters, T., De Pinna, E., Robinson, E., Struthers, K., Webber, M., Catto, A., Dallman,
716 T.J., Hawkey, P., Loman, N.J., 2015. Rapid draft sequencing and real-time nanopore
717 sequencing in a hospital outbreak of *Salmonella*. *Genome Biol* 16, 114.
718 <https://doi.org/10.1186/s13059-015-0677-2>

719 Quinlan, A.R., Hall, I.M., 2010. BEDTools: a flexible suite of utilities for comparing genomic
720 features. *Bioinformatics* 26, 841–842. <https://doi.org/10.1093/bioinformatics/btq033>

721 R Core Team, 2016. R: A Language and Environment for Statistical Computing. R Foundation
722 for Statistical Computing, Vienna.

723 Ramirez-Gonzalez, R., Yu, D.W., Bruce, C., Heavens, D., Caccamo, M., Emerson, B.C., 2013.
724 PyroClean: Denoising Pyrosequences from Protein-Coding Amplicons for the Recovery
725 of Interspecific and Intraspecific Genetic Variation. *PLoS ONE* 8, e57615.
726 <https://doi.org/10.1371/journal.pone.0057615>

727 Reinemeyer, C.R., Nielsen, M.K., 2009. Parasitism and colic. *Vet Clin North Am Equine Pract*
728 25, 233–245. <https://doi.org/10.1016/j.cveq.2009.04.003>

729 Sallé, G., Guillot, J., Tapprest, J., Foucher, N., Sevin, C., Laugier, C., 2020. Compilation of
730 29 years of postmortem examinations identifies major shifts in equine parasite prevalence
731 from 2000 onwards. *Int J Parasitol* 50, 125–132.
732 <https://doi.org/10.1016/j.ijpara.2019.11.004>

733 Sallé, G., Kornáš, S., Basiaga, M., 2018. Equine strongyle communities are constrained by horse
734 sex and species dispersal-fecundity trade-off. *Parasit Vectors* 11, 279.
735 <https://doi.org/10.1186/s13071-018-2858-9>

736 Shen, W., Le, S., Li, Y., Hu, F., 2016. SeqKit: A Cross-Platform and Ultrafast Toolkit for
737 FASTA/Q File Manipulation. *PLoS One* 11, e0163962.
738 <https://doi.org/10.1371/journal.pone.0163962>

739 Srivathsan, A., Baloglu, B., Wang, W., Tan, W.X., Bertrand, D., Ng, A.H.Q., Boey, E.J.H., Koh,
740 J.J.Y., Nagarajan, N., Meier, R., 2018. A MinION™-based pipeline for fast and cost-
741 effective DNA barcoding. *Mol Ecol Resour* 18, 1035–1049.
742 <https://doi.org/10.1111/1755-0998.12890>

743 Torbert, B.J., Klei, T.R., Lichtenfels, J.R., Chapman, M.R., 1986. A survey in Louisiana of
744 intestinal helminths of ponies with little exposure to anthelmintics. *J Parasitol* 72, 926–
745 930.

746 Untergasser, A., Cutcutache, I., Koressaar, T., Ye, J., Faircloth, B.C., Remm, M., Rozen, S.G.,
747 2012. Primer3--new capabilities and interfaces. *Nucleic Acids Res* 40, e115.
748 <https://doi.org/10.1093/nar/gks596>

749 Venables, W.N., Ripley, B.D., 2002. Modern Applied Statistics with S, 4th ed. Springer, New-
750 York.

751 Wang, S., Li, P., Sun, C., Liu, W., Bu, Y., 2020. Complete mitochondrial genome and
752 phylogenetic analysis of *Cyathostomum tetricanthum* (Rhabditida: Cyathostominae).
753 Mitochondrial DNA B Resour 5, 744–745.
754 <https://doi.org/10.1080/23802359.2020.1715289>

755 Workentine, M.L., Chen, R., Zhu, S., Gavriliuc, S., Shaw, N., Rijke, J. de, Redman, E.M.,
756 Avramenko, R.W., Wit, J., Poissant, J., Gilleard, J.S., 2020. A database for ITS2
757 sequences from nematodes. BMC Genet 21, 74. <https://doi.org/10.1186/s12863-020-00880-0>

759 Yang, S., Li, P., Sun, C., Liu, W., 2020. The complete mitochondrial genome of *Coronocyclus*
760 *labratus* (Rhabditida: Cyathostominae). Mitochondrial DNA B Resour 5, 1044–1045.
761 <https://doi.org/10.1080/23802359.2020.1721361>

762

763 **Figure captions**

764

765 **Figure 1. Comparison of the predictive abilities of cyathostomin community structure for**
766 **the mitochondrial COI and ITS-2 rDNA barcodes**

767 Considered coefficient values are represented across three mock community sizes for the
768 mitochondrial COI (blue) and ITS-2 rDNA (yellow) barcodes. F1-score corresponds to the trade-
769 off between identifying true positives while minimizing the false discovery rate (panel A).
770 Divergence was computed as the Bray-Curtis (species relative abundances; panel B) or Jaccard
771 distances (species presence/absence; panel C) between the expected and observed mock
772 community composition. Differences between observed and expected alpha diversity are given in
773 panels D and E. Panel F depicts the fraction of reads with no taxonomy assigned.

774

775 **Figure 2. The relationship between input DNA concentration and observed counts across**
776 **two runs**

777 Recovered species counts for the ITS-2 rDNA (top panels) and COI (bottom row) barcodes are
778 plotted against the respective input DNA concentration before amplification for two replicate
779 samples (left and right panels). Regression slopes of read count upon DNA concentration are
780 represented (black dashed line) and the grey dashed line would fit perfect correlation between
781 input DNA and observed read counts.

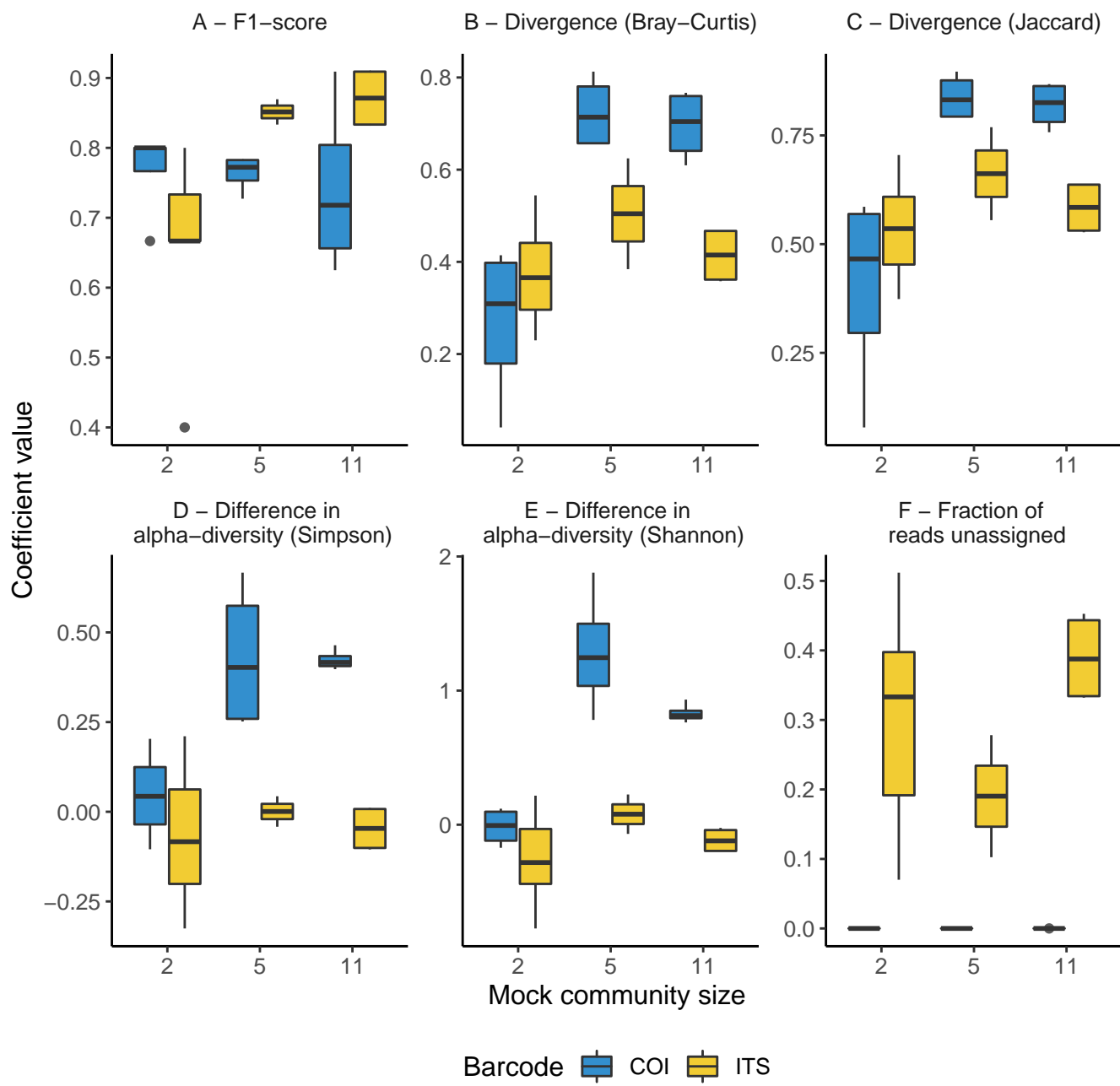
782

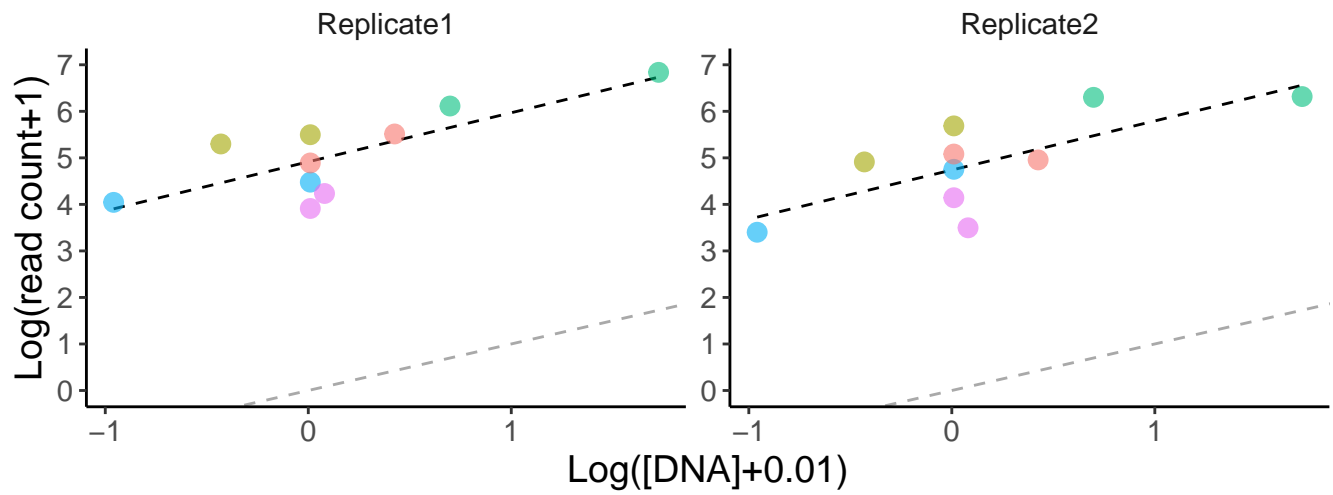
783 **Figure 3. Impact of the considered life-stage on predicted equine strongylid community**
784 **diversity**

785 Panel A provides the relative abundances measured in the strongylid communities from six
786 horses using the COI or ITS-2 barcodes and across three sample types. Panels B and C show the

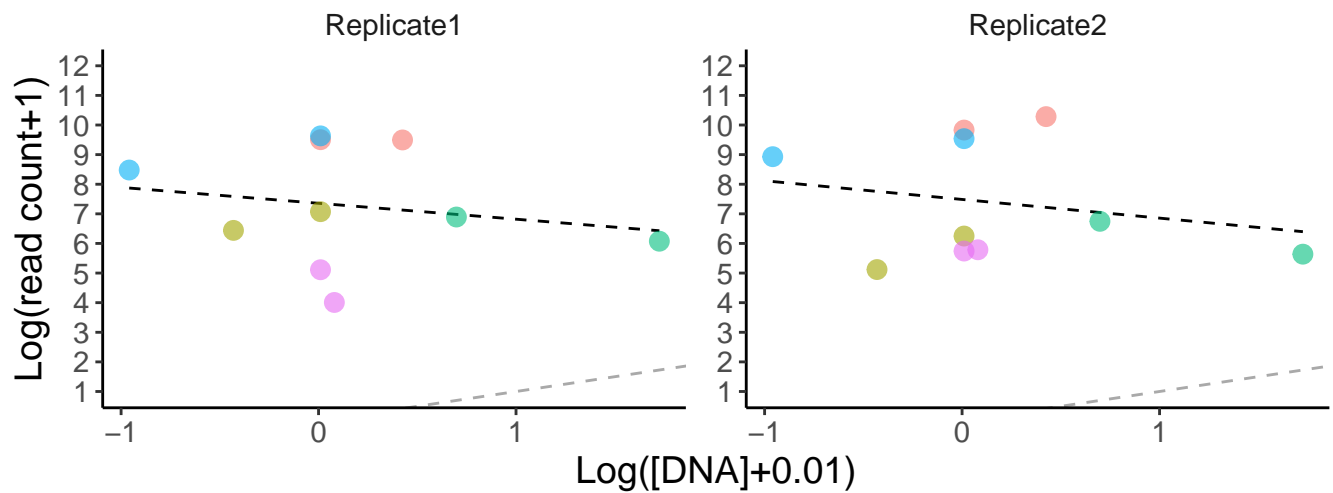
787 first two axes of a Non-linear Multidimensional Scaling analysis based on Bray-Curtis
788 dissimilarity for the COI and ITS-2 rDNA region respectively. The plot illustrates the
789 consistency of species relative abundances across sample types and the reduced alpha diversity
790 for the COI barcode.

791





● Coronocyclus labiatus ● Cyathostomum pateratum ● Cylicocyclus nassatus
● Cyathostomum catinatum ● Cylicocyclus insigne



● Coronocyclus labiatus ● Cyathostomum pateratum ● Cylicocyclus nassatus
● Cyathostomum catinatum ● Cylicocyclus insigne

